JACS
JOURNAL OF THE AMERICAN CHEMICAL SOCIETY
pubs.acs.org/JACS
Article

^{13}C Radiofrequency Amplification by Stimulated Emission of Radiation Threshold Sensing of Chemical Reactions

Andreas B. Schmidt,◊ Isaiah Adelabu,◊ Christopher Nelson,◊ Shiraz Nantogma, Valerij G. Kiselev, Maxim Zaitsev, Abubakar Abdurraheem, Henri de Maissin, Matthew S. Rosen, Sören Lehmkuhl, Stephan Appelt, Thomas Theis,* and Eduard Y. Chekmenev*

Cite This: J. Am. Chem. Soc. 2023, 145, 11121−11129
Read Online
ACCESS | Metrics & More | Article Recommendations | Supporting Information

ABSTRACT: Conventional nuclear magnetic resonance (NMR) enables detection of chemicals and their transformations by exciting nuclear spin ensembles with a radio-frequency pulse followed by detection of the precessing spins at their characteristic frequencies. The detected frequencies report on chemical reactions in real time and the signal amplitudes scale with concentrations of products and reactants. Here, we employ Radiofrequency Amplification by Stimulated Emission of Radiation (RASER), a quantum phenomenon producing coherent emission of ^{13}C signals, to detect chemical transformations. The ^{13}C signals are emitted by the negatively hyperpolarized biomolecules without external radio frequency pulses and without any background signal from other, nonhyperpolarized spins in the ensemble. Here, we studied the hydrolysis of hyperpolarized ethyl-[1-^{13}C]acetate to hyperpolarized [1-^{13}C]acetate, which was analyzed as a model system by conventional NMR and ^{13}C RASER. The chemical transformation of ^{13}C RASER-active species leads to complete and abrupt disappearance of reactant signals and delayed, abrupt reappearance of a frequency-shifted RASER signal without destroying ^{13}C polarization. The experimentally observed "quantum" RASER threshold is supported by simulations.

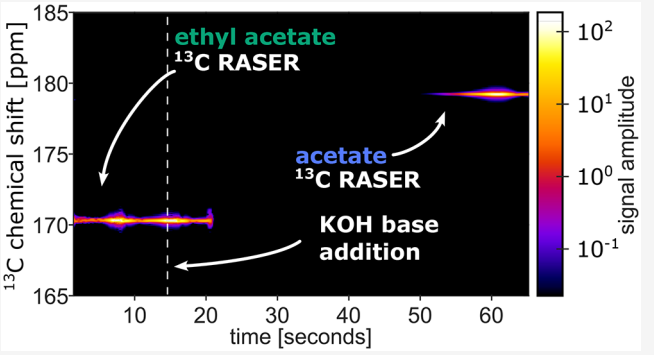

INTRODUCTION

Nuclear magnetic resonance (NMR) offers exquisite sensitivity to the chemical structure and its transformations because small changes in the molecular structure result in sufficiently large changes in nuclear resonance frequencies that can readily be sensed by modern NMR spectrometers and MRI scanners with sub-ppm precision.[1] The technology has excellent deep tissue penetration, and therefore, is "ideally" suited for real-time detection of metabolic transformations.[2] However, the detection sensitivity of conventional MRI technology has been fundamentally impaired because the detected signal relies on the relative population difference of nuclear spin eigenstates, parallel or antiparallel with the magnetic field of the MRI scanner. This population difference is termed nuclear spin polarization P with $P = 0$ for equally populated states and $P = \pm 1$ for complete parallel or antiparallel orientation of the spins. While P increases with the external magnetic field, even at magnetic fields of modern MRI scanners (~3 T), P is only $\sim 10^{-5}$ for protons. Because of this massive sensitivity limitation, detection of low-concentration metabolites in vivo is only possible at the expense of spatial and temporal resolution.[3,4] For instance, a typical magnetic resonance spectroscopic imaging (MRSI) scan takes many minutes with a voxel size of 5 × 5 × 10 mm^3.[5] Unsurprisingly, conventional MRSI is not widely used in clinical practice.

Several approaches have been demonstrated to boost P to the order of unity, i.e., several orders of magnitude above the equilibrium level, to improve NMR detection sensitivity.[6,7] Such hyperpolarized (HP) states are created transiently on small exogenous molecules used as contrast agents that can be injected in vivo to probe metabolic transformations.[8−11] Hyperpolarized ^{13}C-labeled carboxylates are favored because they can retain an HP state for minutes in vivo.[12,13] HP [1-^{13}C]pyruvate is the most developed HP contrast agent,[14−16] and it is now under evaluation in over 30 clinical trials according to clinicaltrials.gov.

Current MRSI detection of HP compounds requires application of radio-frequency (RF) excitation pulses that have to be time-synchronized with magnetic field gradient pulses for image encoding.[6,17−19] The application of RF pulses

Received: January 19, 2023
Published: May 12, 2023

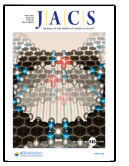

https://doi.org/10.1021/jacs.3c00776
J. Am. Chem. Soc. 2023, 145, 11121−11129

is required to excite the nuclear spins to generating NMR signals in response. Because HP ^{13}C resonates at a frequency vastly different from that of hydrogen atoms (i.e., protons, ^{1}H) detected in conventional MRI, clinical MRI scanners are not equipped for ^{13}C imaging.[18]

Recently, evidence is mounting that the HP state offers one largely unrealized opportunity. Under certain conditions, HP nuclear spin ensembles can emit coherent RF radiation on its own,[20−25] i.e., without RF excitation, which becomes possible due to stimulated emission via Radiofrequency Amplification by Stimulated Emission of Radiation (RASER).[23] The concept of stimulated emission was first introduced by Einstein in his seminal contribution on quantum theory of emission.[26] Decades later, this work laid the foundation for the development of lasers that employ stimulated light emission enabled by population inversion of electronic energy levels. RASER is different from laser in that it employs population inversion of nuclear spin energy levels. As a result, RASER produces emission in the kHz−MHz frequency range, and more importantly, RASER dynamics are often primarily governed by the nuclear spin interactions and can thus directly report on molecular structures and their transformations as we demonstrate here.

In conventional NMR, RASER is not routinely observed for two reasons. First, the nuclear spins in their equilibrium prefer noninverted population distribution, which only leads to radiation damping, not spontaneous RASER. Second, and more importantly, typical equilibrium P of the corresponding energy levels is far below the RASER threshold required for spontaneous emission. Unsurprisingly, the RASER phenomenon[23,27] emerged when achieving near-unity P through hyperpolarization techniques.[6]

RASER presents new opportunities[27−31] including two recent, synergistic advances. First, RASER can be employed for MRI without application of RF excitation pulses.[32] Second, the feasibility of a ^{13}C RASER has been shown.[33] Together, these advances suggest the feasibility of ^{13}C RASER imaging in vivo when using specialized (high-quality factor (Q)) detection electronics, which could be readily compatible with clinical MRI scanners.[33] The potential use of high-Q resonators (not typically employed in conventional proton MRI) is also supported from the perspective of imaging spectral bandwidth since the ^{13}C imaging matrix is typically 1−2 orders of magnitude more sparse than that of protons in each spatial dimension, and a substantially smaller imaging spectral bandwidth is required for ^{13}C image encoding. Therefore, high-Q resonators present a viable technology for HP ^{13}C applications.

However, the capability of the RASER to detect chemical transformations has not been demonstrated, yet it is paramount for any potential biomolecular imaging platform. While both conventional pulsed NMR and RASER employ the same energy levels of nuclear spin to generate the signal, the spin physics behind the stimulated emission is different from that of conventional pulsed NMR.

In this study, we describe the utility of stimulated emission of ^{13}C RASER to detect the hydrolysis of HP ethyl [1-^{13}C]acetate to potassium [1-^{13}C]acetate. Specifically, we show experimentally and theoretically that signal amplitude of the reagent and the product is highly nonlinear with respect to the emission threshold, and virtually, no emission is observed below this threshold. On the other hand, marginally exceeding the RASER threshold results in strong signal emission. This nonlinear sensor behavior is in sharp contrast with conventional pulsed NMR, where the detected signal is directly proportional to the concentration and polarization of detected molecules. We also discuss the advantages and disadvantages of RASER detection in the context of kinetics modeling, sensitivity, and resolution.

RESULTS

^{13}C Hyperpolarization of Ethyl Acetate and Ethyl [1-^{13}C]Acetate. Batches of ^{13}C-hyperpolarized ethyl [1-^{13}C]-acetate at a concentration of 0.5−1 M were produced in CD_3OD using hydrogenative Parahydrogen Induced Polarization (PHIP). The highest ^{13}C polarization (P_{13C}) observed was ≈7% for 0.5 M ethyl [1-^{13}C]acetate as quantified by NMR spectroscopy. The determination of the hyperpolarization level was performed with the nonisotope-enriched compound (≈1.1% ^{13}C isotope fraction) to quantify P_{13C} in the absence of RASER. The longitudinal relaxation time T_1 of the [1-^{13}C] nucleus of 1 M ^{13}C-HP ethyl acetate in CD_3OD at 1.4 T was 72.8 ± 0.1 s, Figure S3.

Hydrogenation and Hydrolysis Reaction Monitoring Using Conventional ^{13}C NMR Spectroscopy. Hydrogenative PHIP is a two-step process. First, pairwise parahydrogen (p-H_2) addition is completed; then, magnetic field cycling (MFC) is employed to transfer polarization from parahydrogen-derived protons to the ^{13}C nucleus, Figure 1A. Because the nascent p-H_2-derived protons have a substantially faster relaxation rate (T_{rel} = 12 ± 2 s) than the ^{13}C, it is imperative to perform the hydrogenation reaction on the time scale of T_{rel} or faster in order to minimize proton-depolarization and to maximize P_{13C}. Hence, the reaction was performed at an elevated temperature (≈67 °C) in CD_3OD and at an elevated pressure (≈8 bar) of p-H_2. The ^{13}C hyperpolarization level of natural-abundance ethyl acetate was measured as a function of hydrogenation time t_h, and the maximum was observed after ∼12 s bubbling time. Kinetic modeling (Figure 1B) and NMR analysis (Figure S1) indicated that most precursor (∼100%) was reacted by 20 s. Based on this kinetic optimization with 0.5 M substrate, all further studies were performed with 1 M substrate concentration, p-H_2 bubbling time of 20 s, and higher temperature (≈88 °C) to ensure complete chemical conversion and maximized ^{13}C polarization.

Upon the addition of potassium hydroxide (KOH, 3 M in 300 μL D_2O) to a sample of ^{13}C-hyperpolarized ethyl acetate (1 M in 600 μL CD_3OD), near-complete cleavage of the ethyl sidearm was observed resulting in the ^{13}C NMR detection of the formed HP acetate (Figure 1C). ^{1}H NMR spectroscopy of the thermally polarized material (acquired approximately 3 min after KOH addition) confirmed almost near complete cleavage (≈90%, Figure S1). The hydrolysis reaction was also monitored by conventional ^{13}C NMR spectroscopy of HP ethyl acetate (Figure S2). As it may be expected, these control experiments revealed the initial presence of HP ethyl acetate before KOH addition. After KOH addition, two ^{13}C NMR lines were observed (corresponding to the HP reagent (ethyl acetate) and the HP product (acetate)). When all reagents were hydrolyzed, only one ^{13}C HP resonance of the acetate product was detected (Figure S2).

^{13}C RASER Detection of HP Ethyl [1-^{13}C]Acetate. As described recently,[33] when the sample of ^{13}C-labeled (99%) ethyl [1-^{13}C]acetate is hyperpolarized in a conventional 5 mm NMR tube and inserted into the detection circuit of a 1.4 T

https://doi.org/10.1021/jacs.3c00776
J. Am. Chem. Soc. 2023, 145, 11121−11129

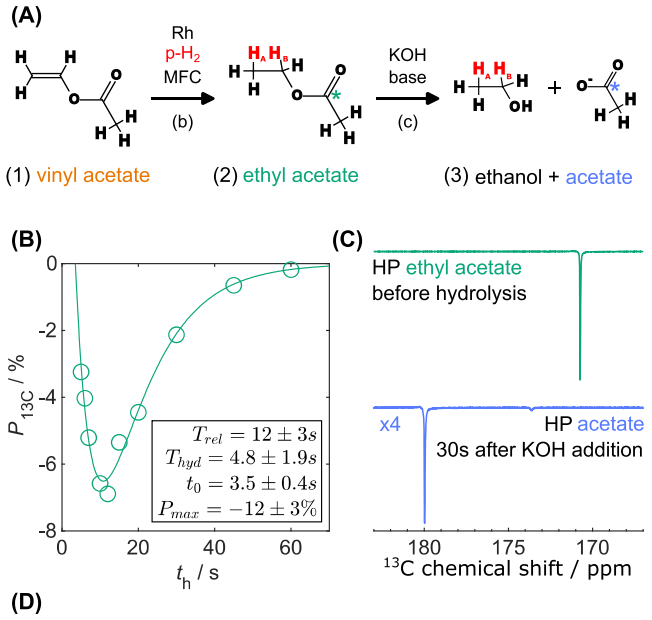

Figure 1. Reaction monitoring with conventional ^{13}C NMR spectroscopy using natural-abundance ^{13}C-hyperpolarized samples. (A) Schematic of the chemical transformations of pairwise para-hydrogen (p-H_2) addition to vinyl acetate resulting in ethyl acetate using the Rh-based catalyst followed by magnetic field cycling (MFC) to transfer p-H_2-derived spin order to the target [1-^{13}C]-nucleus of acetate (indicated with a green asterisk). KOH addition hydrolyzes HP ethyl acetate resulting in production of ethanol and HP acetate (the HP [1-^{13}C] nucleus is indicated with a blue asterisk). (B) Kinetics of ^{13}C PHIP hyperpolarization of ethyl acetate (0.5 M) monitored by conventional ^{13}C and ^{1}H NMR spectroscopy. (C) ^{13}C NMR spectra of HP ethyl acetate before (green trace) and ∼30 s after (blue trace) the start of the hydrolysis reaction with KOH solution. ^{1}H NMR data of the substrates and products from which concentrations were calculated are presented in Figure S1. All presented data were recorded at 15 MHz ^{13}C resonance frequency using a 1.4 T SpinSolve Carbon 60, Magritek spectrometer. (D) Bi-exponential model governing the observed experimental kinetics[33,34] (shown in display B, green circles) of the HP ^{13}C signal as a function of p-H_2 bubbling time (hydrogenation; curve fitting shown by the solid green line).

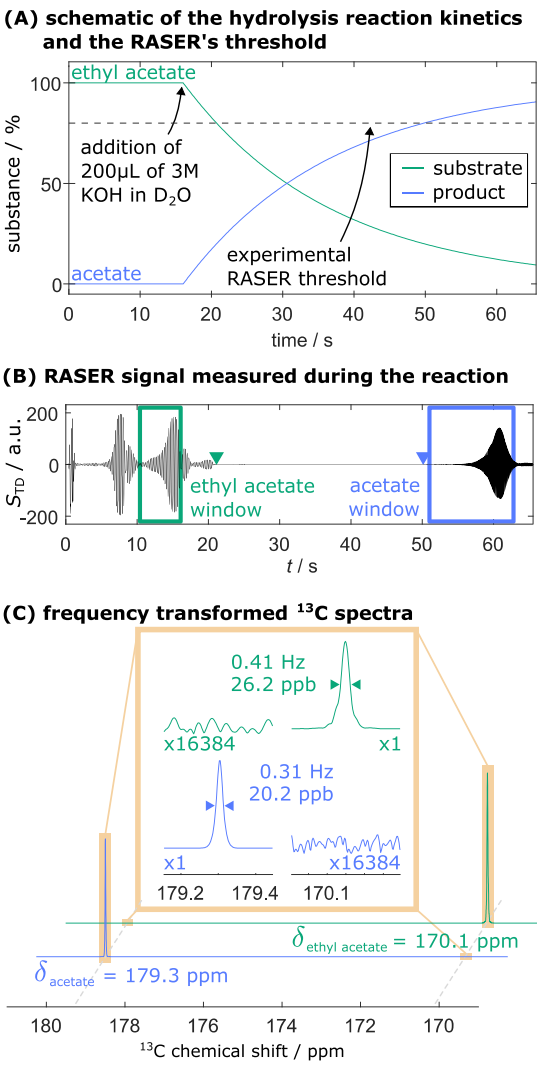

Figure 2. ^{13}C RASER sensing of HP ethyl acetate hydrolysis. (A) Schematic explaining the appearance of ^{13}C RASER signals during the chemical reaction of HP ethyl acetate to acetate. Note that the RASER threshold can potentially be adjusted by the experimental parameters (field homogeneity, Q-factor of the RF detector, etc.). (B) Time-domain ^{13}C RASER signal of the reaction mixture before, during, and after addition of KOH to HP ethyl [1-^{13}C]acetate. (C) Representative FT of the time-domain intervals shown in (B) by green trace, HP ethyl acetate, and blue trace, HP acetate. The ^{13}C RASER spectra were observed at 170.37 ppm (ethyl acetate) and at 179.22 ppm (potassium acetate) with a full width at half maximum (FWHM) of 0.41 and 0.31 Hz, respectively. See the SI for details including Figure S6 discussing the effect of window selection on the spectral profile. The time-domain data presented in display 2B are also presented in the frequency domain, as shown in Figure 3, where individual time windows of the full trace are Fourier-transformed.

spectrometer, spontaneous ^{13}C RASER signals are observed for over 60 s in samples with concentrations as low as 0.12 M. The ^{13}C signal detection time was limited to ≈65 s due to hardware limitations. The representative example of ^{13}C RASER using 0.5 M HP ethyl [1-^{13}C] ethyl acetate is shown in Figure S4. This ^{13}C RASER spectrum contains only one NMR resonance corresponding to ethyl [1-^{13}C]acetate. The ^{13}C RASER signals were obtained using regular NMR hardware provided by the vendor with an RF detector quality factor of 32.

^{13}C RASER Sensing of Ethyl [1-^{13}C]Acetate Hydrolysis to [1-^{13}C]Acetate. In a separate experiment, the HP ethyl [1-^{13}C]acetate (1 M) sample was prepared and inserted into a 1.4 T spectrometer for detection, and 3 M KOH (300 μL D_2O) was added to the sample approximately 17 s after positioning it inside the NMR spectrometer; Figure 2A. In this case, the ^{13}C-RASER signal vanishes within seconds after KOH addition. No ^{13}C NMR signal was detected for approximately 30 s. Remarkably, after 30 s, strong ^{13}C RASER signal suddenly re-appeared; Figure 2B. Careful analysis of the ^{13}C RASER signal in the frequency domain (Figure 2B) confirms that the newly appeared ^{13}C RASER signal resonates at a different frequency, corresponding to the product of hydrolysis, HP [1-^{13}C]acetate; Figure 2C. Overall, the Fourier transform (FT) of the RASER signals before and after addition of base (KOH) revealed narrow ^{13}C NMR signals (with FWHM of 0.31 and 0.41 Hz respectively), separated by approximately 9 ppm (∼135 Hz); Figure 2.

To analyze the observed ^{13}C-RASER signals during the chemical hydrolysis reaction, the following analysis (detailed in

https://doi.org/10.1021/jacs.3c00776
J. Am. Chem. Soc. 2023, 145, 11121−11129

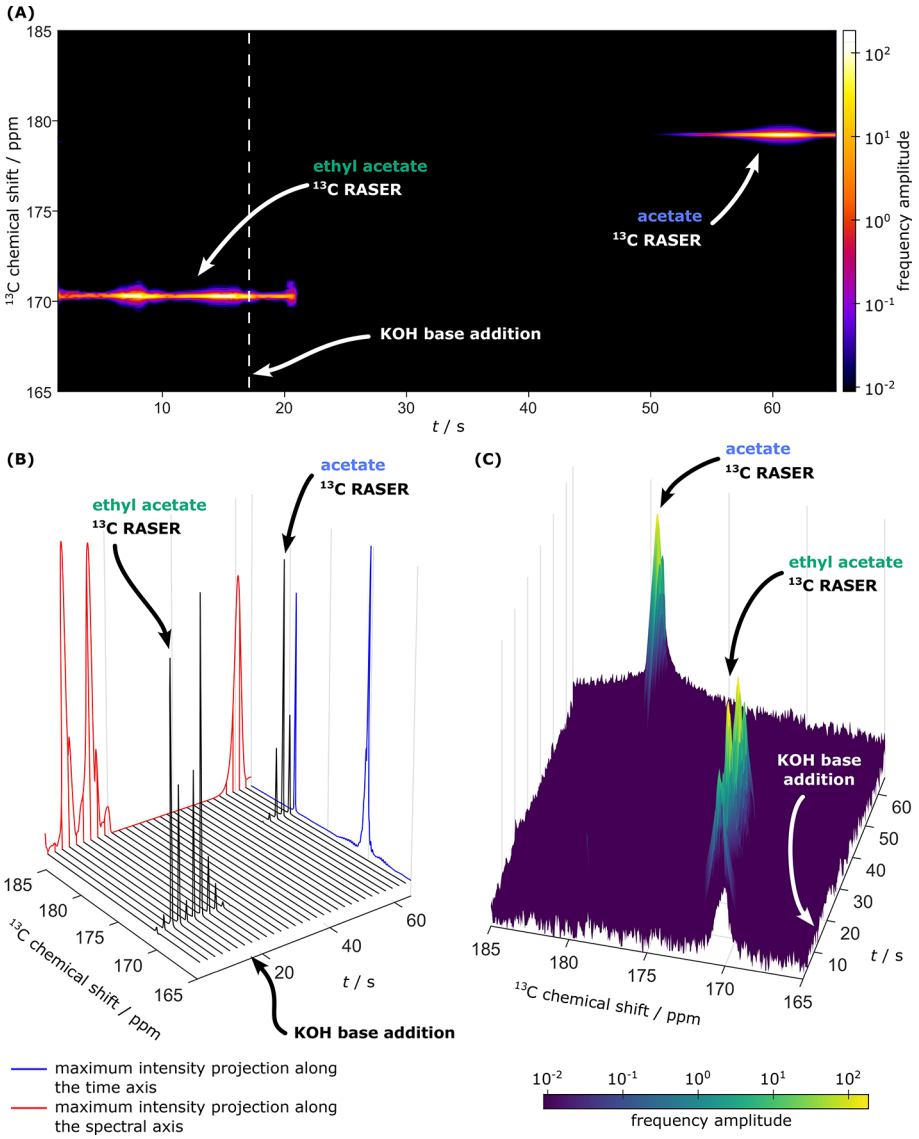

Figure 3. Nonlinear RASER sensing of hydrolysis reaction. (A) FT 2D ^{13}C-RASER (using time-domain data shown in Figure 2B) as a function of frequency and time, showing the high intensity, background-free RASER signals detected from HP ethyl [1-^{13}C]acetate before and from HP [1-^{13}C]acetate after KOH addition. (B) Waterfall plot representation of the ^{13}C RASER data presented in display A showing the maximum intensity projections (selected FT spectra are presented in black to guide the eye). (C) Surface plot of the spectrograph. Note the logarithmic scale in displays A and C, emphasizing low-intensity signals.

the SI and Figures S5−S7) was performed. First, the FT data were reconstructed in 2D as a function of ^{13}C chemical shift and time, clearly showing the RASER signals originating from the two different chemical species (i.e., first ethyl acetate and later acetate); Figure 3A. To this end, one-second intervals of the time domain ^{13}C-RASER data were selected and processed individually to obtain spectral data in the frequency domain (see SI). In other words, the time window (for FT) was shifted along the time dimension; Figure S7. From the obtained 2D frequency domain data (i.e., the spectral information as a function of time), the following was extracted: maximum signal intensity (Figure S7B,C), the FWHM of the observed peak (Figure S7D), and the resonance frequency (Figure S7E). The data produced in this fashion (same data set) are also presented as the waterfall plot along with projections of the maximum intensity in Figure 3B and as a surface diagram in Figure 3C.

DISCUSSION

In general, the RASER effect is generated when large population inversion of a spin system (i.e., $P < 0$) is created, and this spin state interacts with a resonant circuit in a regime where the radiation damping rate exceeds the transverse relaxation rate.[27] The ^{13}C spin system enters the RASER condition when the spin density threshold, n_{th}, is exceeded:[27]

$$n_{th} = -4/(\mu_0 \hbar \cdot \eta \cdot Q \cdot {\gamma_{13C}}^2 \cdot P_{13C} \cdot T_2^*) \quad (1)$$

where μ_0 is the vacuum permeability, $\hbar$ is the Planck's constant, η is the filling factor, Q is the quality factor of the resonator, γ_{13C} is the ^{13}C gyromagnetic ratio, and T_2^* is the effective transverse relaxation time rate constant (≈1.3 s under our conditions).[33] We note that close to this threshold, the signal amplitude is extremely nonlinear with respect to polarization, as detailed below.

https://doi.org/10.1021/jacs.3c00776
J. Am. Chem. Soc. 2023, 145, 11121−11129

Under our experimental conditions (including P_{13C} of ≈7%), n_{th} corresponds to ∼0.1 M ^{13}C substrate concentration.[33] Because the natural ^{13}C abundance is only 1.1%, the natural-abundance HP samples did not exceed n_{th} under our experimental conditions, e.g., ^{13}C spin density n_S corresponded to 0.01 M concentration for 1 M substrate concentration, therefore preventing ^{13}C RASER activity in such natural-abundance HP samples.

In case of 1-^{13}C-labeled HP ethyl [1-^{13}C]acetate, once the 1 M HP sample was inserted into the inductive NMR detector, a ^{13}C RASER is observed because n_S exceeded n_{th}; Figure 2. KOH addition leads to fast depletion of the reagent's spin density n_S, exacerbated additionally by sample dilution. It is also important to note that the reaction rate in our system is substantially faster than the depolarization rate (proportional to $1/T_1$, Figures S2 and S3). Once the reagent's n_S is below n_{th}, the ^{13}C RASER condition for ethyl [1-^{13}C]acetate is no longer fulfilled, resulting in the disappearance of the corresponding ^{13}C RASER signal; Figure 3. Importantly, the ^{13}C RASER signal disappearance is complete despite the residual presence of the HP reagent (Figure S2). The inset of Figure 2C shows no ^{13}C RASER signal of the reagent even under 16,384-fold magnification. This notion is also supported by the dynamic time-resolved ^{13}C RASER data presented in the surface plot with logarithmic scaling, providing four orders of magnification; Figure 3C. Similarly, the initial HP product's n_S build-up does not lead to the observable ^{13}C RASER signal until n_{th} is exceeded; Figures 2 and 3. The experimental data shown in Figures 2 and 3 represent a single data set obtained from the same dynamic run. The presented data were reproduced twice: Figure S8 shows a replicate experiment showing the same trends. Since KOH solution was injected manually at a slightly earlier time (by ∼10 s), the disappearance of the RASER signal from the reagent and the appearance of the RASER signal from the product molecule are shifted in the acquisition window; however, the time gap between the disappearance of the RASER signal from the reagent and the appearance of the RASER signal from the product molecule is similar in both replicate experiments, clearly demonstrating reproducibility of the presented results. Moreover, three additional experiments performed with suboptimal reaction rates revealed the overall delay in the appearance of the RASER signal from the product molecule since more time was required to create a sufficiently high product concentration to exceed the RASER threshold (Figure S9). These additional runs support the key findings presented in this work.

The experimental observations are also supported by simulations; Figure 4. A recently developed simulation approach[33] was applied to investigate ^{13}C RASER signal dependence as a function of population inversion. Virtually, no signal is observed below the RASER threshold (10^{10} spins in a 5 mm NMR tube are well below any usual NMR detection limit). Note the logarithmic scale shown in the inset, illustrating that the RASER signal increases by more than six orders of magnitude over a region where the population inversion only grows by 20%, right after surpassing the RASER threshold. Thus, unlike in conventional HP ^{13}C sensing, where the signal is directly proportional to n_S (Figure S2), the ^{13}C RASER signal behavior of the spin system is highly nonlinear, and ^{13}C RASER effectively acts as a quantum filter or a gate, for selective sensing of polarized molecules that are used in this demonstration for real-time reaction monitoring. While the RASER threshold simulation is the result of solving a set of classical differential equations, the observed behavior is also reminiscent of the quantum effects such as the photoelectric effect, where electron emission is only observed above a given wavelength of the light hitting the surface.

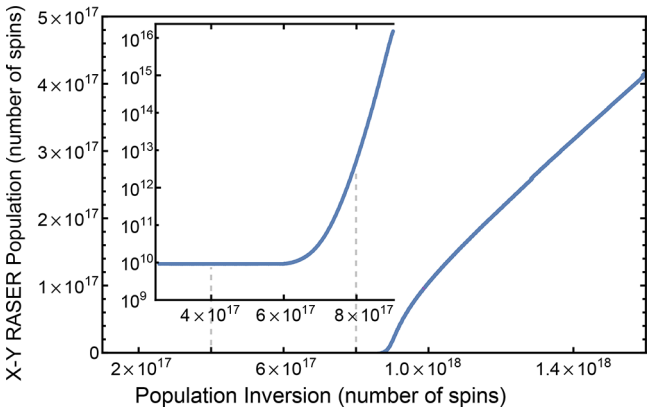

Figure 4. Simulations of ^{13}C RASER signal dependence on the population inversion. The inset shows the selected region of logarithmic scaling to emphasize the near zero signal below the threshold level. Notice that 10^{10} spins in the transverse plane are used to induce spontaneous stimulated emission. The following parameters are chosen in the simulation to approximately reflect the experiment: ω_0 = 15 MHz, γ_{13C} = 10.7 MHz/T, V_s = 0.1 mL, $\hbar$ = 1.054571817 × 10^{-34} J/Hz, μ_0 = 1.2566370621 × 10^{-6} J/(A^2 m), Q = 32, T_2* = 1.4 s, and T_1 = 66 s. The simulation also includes a small additional pumping term given as $\Gamma = 0.1\ e^{-t/60}$, which is required to include the experimentally observed RASER bursts. With all these parameters, the factor g_m and κ_m were calculated as $g_m = \sqrt{(\mu_0 \cdot \hbar \cdot \gamma_{13C} \cdot \omega_0 / 4V_S)}$ and $\kappa_m = \omega_0/Q$. Next, with those parameters, it is then possible to estimate the population inversion threshold, d_{th}, for RASER as $d_{th} = \kappa_m/(g_m^2 \cdot T_2^*)$, which results as 5.88 × 10^{17} spins.

Similarly, the simulations also reveal one other important RASER feature: once the RASER threshold is exceeded significantly (by more than 30%), the signal scales linearly with population inversion; this behavior also appears similar to the field-effect transistor (FET) current−voltage characteristics. In FET, maintaining the gate voltage below the switching threshold level keeps the transistor channel in the "off" position, whereas exceeding this voltage switches the transistor channel "on" to the linear current−voltage region.

The simulation shown in Figure 4 reveals that transverse, $X-Y$ population does not exceed the initial population inversion. This clearly indicates that the NMR signal obtained via RASER does not exceed the conventional NMR signal under otherwise identical conditions. However, since RASER signal acquisition may continue well beyond the T_2* limit,[28] it is possible for RASER detection to exceed the sensitivity of conventional NMR detection using RF excitation pulses via effective line narrowing observed in the ^{13}C RASER.[33] Future simulations and experimental studies are certainly warranted in this direction. Moreover, ^{13}C RASER detection certainly offers an advantage in the context of spectral resolution as it fundamentally allows signal acquisition well beyond the T_2* limit of conventional NMR detection. As indicated in the simulations of Figure 4, RASER activity can include quasi linear regimes above the RASER threshold. Especially in the case of a single, well-defined resonance frequency, quasi linear behavior can be used for kinetic modeling. However, in the presence of multiple resonances, frequency pulling, intermittence, and even chaos can emerge, complicating chemical kinetics modeling.[28]

https://doi.org/10.1021/jacs.3c00776
J. Am. Chem. Soc. 2023, 145, 11121−11129

This study reports on a significant demonstration of ^{13}C RASER sensing mechanism under nonfavorable conditions, which were dictated by the use of commercially available hardware, which is optimized for conventional NMR rather than for RASER detection. Specifically, n_{th} can be reduced by several orders of magnitude through the use of high-Q detectors. Q values of over 500 were reported for low-frequency applications using external high-quality-factor enhancement (EHQE)[35] or super-conducting NMR detectors.[36,37] Moreover, the use of parametric pumping of the MR detector could boost Q to over 10^5 even at high frequencies. A Q_s value of over 18,000 has been achieved at clinically relevant ^{13}C frequencies of 63 MHz.[38] Finally, the addition of concentrated KOH in D_2O likely resulted in T_2* reduction (observed as line broadening in non-RASER ^{13}C spectra, Figure S2) that transiently increased n_{th} during the RASER reaction monitoring experiment. Addressing the abovementioned limitation is beyond the scope of this pilot report and will require developing novel RASER sensors for this next-generation molecular imaging technique.

We envision the following key advantages of ^{13}C RASER metabolic sensing in the context of potential future in vivo applications. First and foremost, the vast majority (>99.5%) of clinical MRI scanners lack ^{13}C excitation capabilities. As a result, detection of ^{13}C hyperpolarized contrast agents cannot be readily performed on those clinical MRI scanners. Because the RASER detection does not require RF pulses for excitation, it follows that unlike conventional NMR detection, employing RF excitation pulses ^{13}C RASER detection can be performed on any clinical MRI scanner equipped with custom-high-Q sensors. This new approach has the potential to enable a widespread use of HP ^{13}C contrast agents as a next-generation molecular imaging modality.

CONCLUSIONS

To conclude, we have demonstrated that ^{13}C RASER can be employed for selective, highly nonlinear "quantum" sensing of chemical transformations, paving the way to new applications of magnetic resonance, including democratization of access to next-generation molecular imaging technology of HP ^{13}C MRI on a wide range of clinical MRI scanners.

MATERIALS AND METHODS

Objectives and Design of the Study. The overall aim of this work was to investigate and demonstrate nonlinear RASER sensing of chemical reactions. To this end, highly concentrated, ^{13}C-hyperpolarized samples were prepared using parahydrogen-induced polarization (PHIP) and magnetic field cycling (MFC) transferring the spin order to ^{13}C nucleus, where RASER was observable in a benchtop NMR instrument. During RASER activity, a hydrolysis reaction of HP ethyl [1-^{13}C]acetate was induced, which was tracked by the nonlinear RASER threshold.

Sample Preparation. Molecular, gaseous hydrogen was enriched in the nuclear spin singlet state, i.e., parahydrogen, to >99.10% (quantified by benchtop NMR spectroscopy) and stored in aluminum cylinders at 23 bar using a previously described setup.[39] Fresh p-H_2 was prepared on each experiment day. For the PHIP reactions, samples were prepared in methanol-d_4 (CD_3OD, Sigma-Aldrich S/N 151947) using a rhodium-based catalyst (1,4-bis-(diphenylphosphino)butane(1,5-cyclooctadiene)rhodium(I) tetrafluoroborate ([Rh(dppb)(COD)]BF_4), Strem 45-0190, CAS 79255-71-3) at 10 mM concentration and ethyl acetate precursors (vinyl acetate, either natural abundance (Sigma-Aldrich S/N V1503-1L) at a concentration of 0.5 or 1 M, Figure 1, or 1-^{13}C enriched to 99%, custom-synthesized, as described previously;[40] (Figures 2 and 3).

Experimental Setup. A previously described setup was employed for all studies;[41−43] Figure 5. It is composed of (i) a 3-layer mu-metal shield (3″ inner diameter and 9″ length, S/N ZG-203, Magnetic Shield Corp., Bensenville, IL) to reach nanotesla magnetic fields required for the MFC, (ii) a fluidic setup to control the flow of p-H_2 and to guide it through the reaction solution held in the NMR tube,

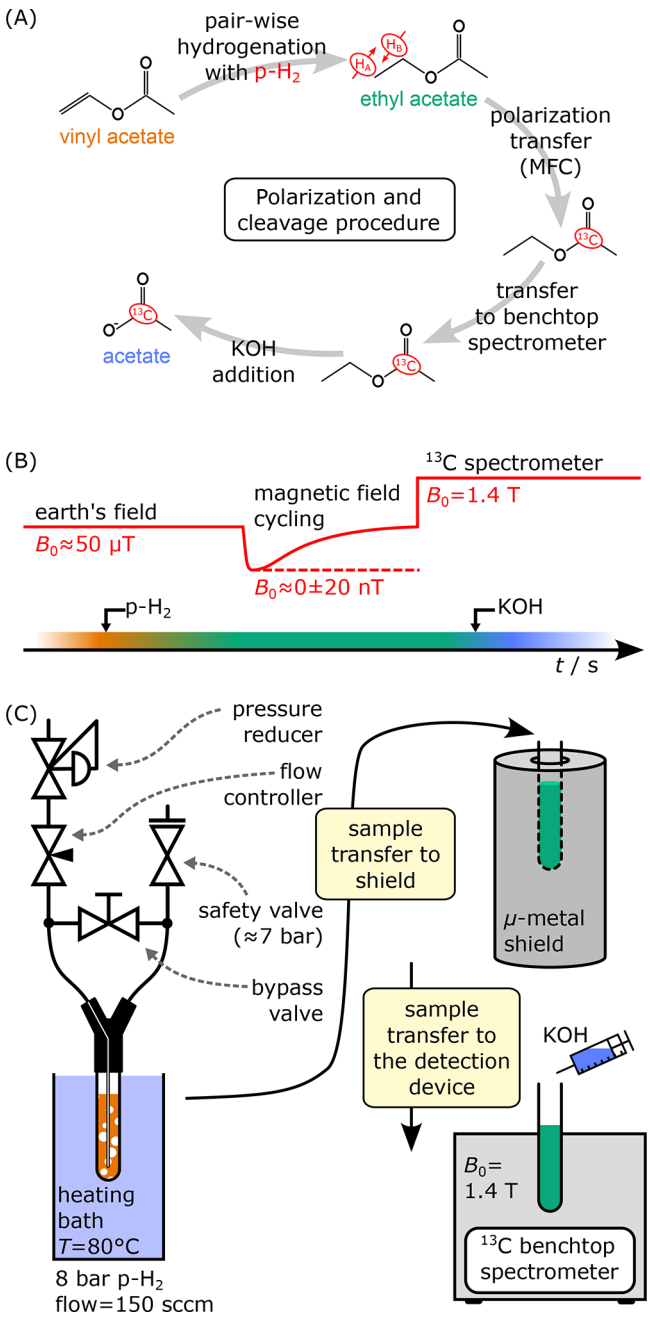

Figure 5. Schematic of the experiment and setup. (A) Multi-step procedure consisting of the p-H_2 bubbling to conduct vinyl acetate hydrogenation, magnetic field cycling for ^{13}C polarization, sample transfer, and KOH base addition; [1-^{13}C]-labeled (99%) hydrogenation substrate was employed for RASER studies, and the natural abundance (1.1% ^{13}C) hydrogenation substrate was used for non-RASER studies. (B) Sequences of the corresponding events. (C) Schematic of experimental setup for p-H_2 pairwise addition to unsaturated substrate, polarization transfer to the ^{13}C nucleus via magnetic field cycling, and RASER quantum sensing of chemical reactions at 1.4 T.

https://doi.org/10.1021/jacs.3c00776
J. Am. Chem. Soc. 2023, 145, 11121−11129

and (iii) an $^{1}H-^{13}C$ 1.4 T benchtop NMR system[42] (Carbon 60, Magritek), which was employed for NMR and RASER detection.

PHIP Experiments. Reaction solutions (600 μL) were filled into 5 mm NMR tubes, which were connected to the fluidic setup. The tube was pressurized with p-H_2 to 8 bar total pressure using a 7 bar overpressure regulated safety valve. The sample was positioned in a water bath that was heated on a hot plate to ∼67 °C for 0.5 M samples (data shown in Figure 1B) or ≈88 °C (all other data). The residual magnetic field at the sample position inside the shield was 0 ± 20 nT after compensating the residual field in the shields (0.12 μT) with a solenoid coil. After equilibrating the temperature of the sample for 35 s in the water bath, p-H_2 was guided through the solution (still being held in the hot water) for 20 s (unless stated otherwise) at a flow rate of 150 standard cubic centimeters per minute (scc/m) using a digital mass flow controller. Subsequently, the sample was quickly (i.e., diabatically within <1 s) moved into the mu-metal shield and slowly (i.e., adiabatically within 3−5 s) taken out of the shield to perform the magnetic field cycle to transfer the p-H_2-derived proton spin order to carbon-13. Notably, this procedure results in an inverted ^{13}C hyperpolarization, where most of the product ethyl [1-^{13}C]acetate populates the higher carbon energy state (referred to as beta or spin-down state). Two effects are present during this process:[33,34] hydrogenation, which forms proton polarization of nascent parahydrogen-derived protons with time constant T_{hyd} and relaxation of the nascent singlet spin order T_{rel}. The hydrogenation process leads to the overall build-up of the proton HP pool, whereas relaxation results in an exponential decrease of the HP state. If no relaxation was present, P_{max} would be reached at time substantially longer than T_{hyd}. Hydrogenation starts with an offset t_0 which reflects finite time needed for p-H_2 to enter, pressure build up, and to dissolve in the solvent; Figures 1 and 4.

^{13}C RASER and NMR Spectroscopy. The sample was transferred into the benchtop 1.4 T NMR spectrometer (Spinsolve 60 Carbon, Magritek) placed next to the mu-metal setup. For conventional ^{13}C NMR spectroscopy, a 90° excitation pulse was applied followed by detection of the free induction decay with ^{1}H decoupling. For the detection of the ^{13}C-RASER (using a bolus of HP 1-^{13}C-enriched ethyl [1-^{13}C]acetate), no ^{13}C excitation pulse was applied and WALTZ (Wideband, alternating-phase, low-power technique for zero residual splitting) ^{1}H decoupling was applied. Proton decoupling was important to lower the RASER threshold via the collapse of the multiplet into a single resonance line. The pulse sequence was started shortly before inserting the sample into the magnet and the resonator. The acquisition duration was limited to 65 s by the software of the NMR spectrometer.

Hydrolysis Reaction. To induce the hydrolysis of HP ethyl acetate to form acetate, the NMR tube was rapidly depressurized, opened, and ≈200 μL of 3 M KOH in D_2O were injected from the top into the HP sample while it was held in the bore of the 1.4 T NMR spectrometer. The sample was mixed for 5 s by bubbling p-H_2 through the solution at a low flow rate of ≈5 scc/m. The RASER data acquisition of the hydrolysis reaction was reproducible (n = 2). Moreover, the experimental data presented here for hydrolysis RASER sensing were additionally repeated for n = 3 at slightly different KOH concentrations (1.5, 2.25, or 6.0 M in 200 μL of D_2O). However, since the use of lower KOH concentrations (1.5 and 2.25 M) likely resulted in the overall slower reaction kinetics, the appearance of the RASER signal from the product molecule was delayed (Figure S9). Therefore, a second acquisition of ∼65 s was needed to fully capture the RASER signal from the product molecule. The use of 6.0 M KOH concentration has led to partial precipitation of the hydrogenation catalyst and likely also resulted in the overall slower kinetics. Indeed, the appearance of the corresponding RASER signal from the product molecule was also delayed (Figure S9).

Conventional ^{13}C NMR Experiments. NMR spectra were acquired using hard excitation RF pulse with decoupling during acquisition. All conventional NMR experiments were performed with the natural-abundance hydrogenation substrate. Time domain NMR signals were Fourier-transformed (FFT algorithm) and phase-corrected, and real components of the NMR spectra are plotted. The ^{13}C hyperpolarization level was quantified by comparing ^{13}C signals of the HP compound with a thermally polarized ^{13}C signal reference (17.5 M 99% 1-^{13}C-enriched neat [1-^{13}C]acetic acid).

^{13}C RASER Studies. From the time domain RASER signal, time intervals were selected and processed (see the SI for more details). In short, a Hann filter function was multiplied to the selected data that were then zero-filled and Fourier-transformed to obtain frequency domain data. The data were corrected for drifts of the magnets field; Figure S5. From the magnitude spectra, the signal intensity, FWHM, and resonance frequency were determined, Figure S7.

■ ASSOCIATED CONTENT

Supporting Information

The Supporting Information is available free of charge at https://pubs.acs.org/doi/10.1021/jacs.3c00776.

Additional details of ^{13}C RASER data processing; SABER hyperpolarization studies; and details of synthesis and spectral characterization (PDF)

■ AUTHOR INFORMATION

Corresponding Authors

Thomas Theis − *Department of Chemistry, North Carolina State University, Raleigh, North Carolina 27695, United States; Department of Physics and Joint UNC & NC State Department of Biomedical Engineering, North Carolina State University, Raleigh, North Carolina 27606, United States;* orcid.org/0000-0001-6779-9978; Email: ttheis@ncsu.edu

Eduard Y. Chekmenev − *Department of Chemistry, Integrative Bio-Sciences (Ibio), Karmanos Cancer Institute (KCI), Wayne State University, Detroit, Michigan 48202, United States; Russian Academy of Sciences, Moscow 119991, Russia;* orcid.org/0000-0002-8745-8801; Email: chekmenevlab@gmail.com

Authors

Andreas B. Schmidt − *Department of Chemistry, Integrative Bio-Sciences (Ibio), Karmanos Cancer Institute (KCI), Wayne State University, Detroit, Michigan 48202, United States; Division of Medical Physics, Department of Radiology, Medical Center, Faculty of Medicine, University of Freiburg, Freiburg 79106, Germany; German Cancer Consortium (DKTK), Partner Site Freiburg and German Cancer Research Center (DKFZ), Heidelberg 69120, Germany;* orcid.org/0000-0001-8944-7463

Isaiah Adelabu − *Department of Chemistry, Integrative Bio-Sciences (Ibio), Karmanos Cancer Institute (KCI), Wayne State University, Detroit, Michigan 48202, United States;* orcid.org/0000-0002-9475-0851

Christopher Nelson − *Department of Chemistry, North Carolina State University, Raleigh, North Carolina 27695, United States*

Shiraz Nantogma − *Department of Chemistry, Integrative Bio-Sciences (Ibio), Karmanos Cancer Institute (KCI), Wayne State University, Detroit, Michigan 48202, United States*

Valerij G. Kiselev − *Division of Medical Physics, Department of Radiology, Medical Center, Faculty of Medicine, University of Freiburg, Freiburg 79106, Germany*

Maxim Zaitsev − *Division of Medical Physics, Department of Radiology, Medical Center, Faculty of Medicine, University of Freiburg, Freiburg 79106, Germany*

Abubakar Abdurraheem − *Department of Chemistry, Integrative Bio-Sciences (Ibio), Karmanos Cancer Institute*

(KCI), Wayne State University, Detroit, Michigan 48202, United States

Henri de Maissin − *Division of Medical Physics, Department of Radiology, Medical Center, Faculty of Medicine, University of Freiburg, Freiburg 79106, Germany; German Cancer Consortium (DKTK), Partner Site Freiburg and German Cancer Research Center (DKFZ), Heidelberg 69120, Germany*

Matthew S. Rosen − *Massachusetts General Hospital, A. A. Martinos Center for Biomedical Imaging, Boston, Massachusetts 02129, United States; Department of Physics, Harvard University, Cambridge, Massachusetts 02138, United States*

Sören Lehmkuhl − *Institute of Microstructure Technology, Karlsruhe Institute of Technology, Karlsruhe 76344, Germany;* orcid.org/0000-0002-1321-7677

Stephan Appelt − *Institute of Technical and Macromolecular Chemistry, RWTH Aachen University, Aachen 52056, Germany; Central Institute for Engineering, Electronics and Analytics—Electronic Systems (ZEA-2), Forschungszentrum Jülich GmbH, Jülich D-52425, Germany*

Complete contact information is available at: https://pubs.acs.org/10.1021/jacs.3c00776

Author Contributions

◊A.B.S., I.A., and C.N. contributed equally to this work.

Notes

The authors declare the following competing financial interest(s): T.T. is a founder, equity holder, and president of Vizma Life Sciences LLC (VLS). M.S.R. is a founder and equity holder of VLS. E.Y.C. declares a stake of ownership in XeUS Technologies Ltd. E.Y.C. serves on the scientific advisory board of VLS. M.S.R. is a founder and equity holder of Hyperfine Inc. All other authors declare that they have no competing interest.

■ ACKNOWLEDGMENTS

This work was supported by the National Institutes of Health grant R21EB025313 (T.T.), R01EB029829 (T.T.), R21 HL154032 (E.Y.C.), National Science Foundation grant: CHE-1904780 (E.Y.C.), WSU Thomas C. Rumble University Graduate Fellowship (S.N. and I.A.), the German Cancer Consortium (DKTK) (A.B.S.), WSU Competition for Postdoctoral Fellow award (A.B.S.), B.E.S.T. Fluidsysteme GmbH I Swagelok Stuttgart (A.B.S.), the German Research Foundation (DFG) grants: #SCHM 3694/1-1, #SCHM 3694/2-1, and #SFB1479 (A.B.S.), the German Federal Ministry of Education and Research (BMBF) in the funding program "Quantum Technologies—from Basic Research to Market" under the project "QuE-MRT" (contract number: 13N16448). M.S.R. acknowledges the generous support of the Kiyomi and Ed Baird MGH Research Scholar award. The content is solely the responsibility of the authors and does not necessarily represent the official views of the National Institutes of Health. This material is based upon work supported by the U.S. Department of Energy, Office of Biological and Environmental Research (BER) under Award Number(s) DE-SC0023334. Disclaimer: This report was prepared as an account of work sponsored by an agency of the United States Government. Neither the United States Government nor any agency thereof, nor any of their employees, makes any warranty, express or implied, or assumes any legal liability or responsibility for the accuracy, completeness, or usefulness of any information, apparatus, product, or process disclosed, or represents that its use would not infringe privately owned rights. Reference herein to any specific commercial product, process, or service by trade name, trademark, manufacturer, or otherwise does not necessarily constitute or imply its endorsement, recommendation, or favoring by the United States Government or any agency thereof. The views and opinions of authors expressed herein do not necessarily state or reflect those of the United States Government or any agency.

■ REFERENCES

(1) Pfeuffer, J.; Tkac, I.; Provencher, S. W.; Gruetter, R. Toward an in vivo neurochemical profile: Quantification of 18 metabolites in short-echo-time H-1 NMR spectra of the rat brain. *J. Magn. Reson.* **1999**, *141*, 104−120.

(2) Bluml, S.; Moreno-Torres, A.; Shic, F.; Nguy, C. H.; Ross, B. D. Tricarboxylic acid cycle of glia in the in vivo human brain. *NMR Biomed.* **2002**, *15*, 1−5.

(3) van der Graaf, M. In vivo magnetic resonance spectroscopy: basic methodology and clinical applications. *Eur. Biophys. J.* **2010**, *39*, 527−540.

(4) Kurhanewicz, J.; Vigneron, D. B.; Hricak, H.; Narayan, P.; Carroll, P.; Nelson, S. J. Three-dimensional H-1 MR spectroscopic imaging of the in situ human prostate with high (0.24-0.1-cm^3) spatial resolution. *Radiology* **1996**, *198*, 795−805.

(5) Dorrius, M. D.; Pijnappel, R. M.; Jansen-van der Weide, M. C.; Jansen, L.; Kappert, P.; Oudkerk, M.; Sijens, P. E. Determination of Choline Concentration in Breast Lesions: Quantitative Multivoxel Proton MR Spectroscopy as a Promising Noninvasive Assessment Tool to Exclude Benign Lesions. *Radiology* **2011**, *259*, 695−703.

(6) Nikolaou, P.; Goodson, B. M.; Chekmenev, E. Y. NMR Hyperpolarization Techniques for Biomedicine. *Chem. − Eur. J.* **2015**, *21*, 3156−3166.

(7) Kovtunov, K. V.; Pokochueva, E. V.; Salnikov, O. G.; Cousin, S.; Kurzbach, D.; Vuichoud, B.; Jannin, S.; Chekmenev, E. Y.; Goodson, B. M.; Barskiy, D. A.; Koptyug, I. V. Hyperpolarized NMR: d-DNP, PHIP, and SABRE. *Chem. − Asian J.* **2018**, *13*, 1857−1871.

(8) Chowdhury, R.; Mueller, C. A.; Smith, L.; Gong, F.; Papoutsaki, M.-V.; Rogers, H.; Syer, T.; Singh, S.; Brembilla, G.; Retter, A.; et al. Quantification of Prostate Cancer Metabolism Using 3D Multiecho bSSFP and Hyperpolarized [1-^{13}C] Pyruvate: Metabolism Differs Between Tumors of the Same Gleason Grade. *J. Magn. Reson. Imaging* **2022**, DOI: 10.1002/jmri.28467.

(9) Golman, K.; in't Zandt, R.; Thaning, M. Real-time metabolic imaging. *Proc. Natl. Acad. Sci. U. S. A.* **2006**, *103*, 11270−11275.

(10) Merritt, M.; Harrison, C.; Storey, C.; Jeffrey, F.; Sherry, A.; Malloy, C. Hyperpolarized C-13 allows a direct measure of flux through a single enzyme-catalyzed step by NMR. *Proc. Natl. Acad. Sci. U. S. A.* **2007**, *104*, 19773−19777.

(11) Day, S. E.; Kettunen, M. I.; Gallagher, F. A.; Hu, D. E.; Lerche, M.; Wolber, J.; Golman, K.; Ardenkjaer-Larsen, J. H.; Brindle, K. M. Detecting tumor response to treatment using hyperpolarized C-13 magnetic resonance imaging and spectroscopy. *Nat. Med.* **2007**, *13*, 1382−1387.

(12) Kurhanewicz, J.; Bok, R.; Nelson, S. J.; Vigneron, D. B. Current and potential applications of clinical C-13 MR spectroscopy. *J. Nucl. Med.* **2008**, *49*, 341−344.

(13) Kurhanewicz, J.; Vigneron, D. B.; Brindle, K.; Chekmenev, E. Y.; Comment, A.; Cunningham, C. H.; DeBerardinis, R. J.; Green, G. G.; Leach, M. O.; Rajan, S. S.; Rizi, R. R.; Ross, B. D.; Warren, W. S.; Malloy, C. R. Analysis of Cancer Metabolism by Imaging Hyperpolarized Nuclei: Prospects for Translation to Clinical Research. *Neoplasia* **2011**, *13*, 81−97.

(14) Chung, B. T.; Chen, H.-Y.; Gordon, J.; Mammoli, D.; Sriram, R.; Autry, A. W.; Le Page, L. M.; Chaumeil, M. M.; Shin, P.; Slater, J.; Tan, C. T.; Suszczynski, C.; Chang, S.; Li, Y.; Bok, R. A.; Ronen, S. M.; Larson, P. E. Z.; Kurhanewicz, J.; Vigneron, D. B. First

hyperpolarized [2-^{13}C]pyruvate MR studies of human brain metabolism. *J. Magn. Reson.* **2019**, *309*, No. 106617.
(15) Kurhanewicz, J.; Vigneron, D. B.; Ardenkjaer-Larsen, J. H.; Bankson, J. A.; Brindle, K.; Cunningham, C. H.; Gallagher, F. A.; Keshari, K. R.; Kjaer, A.; Laustsen, C.; et al. Hyperpolarized ^{13}C MRI: Path to Clinical Translation in Oncology. *Neoplasia* **2019**, *21*, 1−16.
(16) Brindle, K. M. Imaging Metabolism with Hyperpolarized ^{13}C-Labeled Cell Substrates. *J. Am. Chem. Soc.* **2015**, *137*, 6418−6427.
(17) Albers, M. J.; Bok, R.; Chen, A. P.; Cunningham, C. H.; Zierhut, M. L.; Zhang, V. Y.; Kohler, S. J.; Tropp, J.; Hurd, R. E.; Yen, Y.-F.; Nelson, S. J.; Vigneron, D. B.; Kurhanewicz, J. Hyperpolarized C-13 Lactate, Pyruvate, and Alanine: Noninvasive Biomarkers for Prostate Cancer Detection and Grading. *Cancer Res.* **2008**, *68*, 8607−8615.
(18) Yen, Y. F.; Kohler, S. J.; Chen, A. P.; Tropp, J.; Bok, R.; Wolber, J.; Albers, M. J.; Gram, K. A.; Zierhut, M. L.; Park, I.; Zhang, V.; Hu, S.; Nelson, S. J.; Vigneron, D. B.; Kurhanewicz, J.; Dirven, H.; Hurd, R. E. Imaging Considerations for In Vivo C-13 Metabolic Mapping Using Hyperpolarized C-13-Pyruvate. *Magn. Reson. Med.* **2009**, *62*, 1−10.
(19) Larson, P. E. Z.; Bok, R.; Kerr, A. B.; Lustig, M.; Hu, S.; Chen, A. P.; Nelson, S. J.; Pauly, J. M.; Kurhanewicz, J.; Vigneron, D. B. Investigation of tumor hyperpolarized [1-^{13}C]-pyruvate dynamics using time-resolved multiband RF excitation echo-planar MRSI. *Magn. Reson. Med.* **2010**, *63*, 582−591.
(20) Bear, D.; Chupp, T. E.; Cooper, K.; DeDeo, S.; Rosenberry, M.; Stoner, R. E.; Walsworth, R. L. Improved frequency stability of the dual-noble-gas maser. *Phys. Rev. A* **1998**, *57*, 5006−5008.
(21) Chen, H.-Y.; Lee, Y.; Bowen, S.; Hilty, C. Spontaneous emission of NMR signals in hyperpolarized proton spin systems. *J. Magn. Reson.* **2011**, *208*, 204−209.
(22) Hope, M. A.; Björgvinsdóttir, S.; Grey, C. P.; Emsley, L. A Magic Angle Spinning Activated ^{17}O DNP Raser. *J. Phys. Chem. Lett.* **2021**, *12*, 345−349.
(23) Suefke, M.; Lehmkuhl, S.; Liebisch, A.; Blumich, B.; Appelt, S. Para-hydrogen raser delivers sub-millihertz resolution in nuclear magnetic resonance. *Nat. Phys.* **2017**, *13*, 568−572.
(24) Pravdivtsev, A. N.; Sönnichsen, F. D.; Hövener, J.-B. Continuous Radio Amplification by Stimulated Emission of Radiation using Parahydrogen Induced Polarization (PHIP-RASER) at 14 Tesla. *ChemPhysChem* **2020**, *21*, 667−672.
(25) Joalland, B.; Ariyasingha, N. M.; Lehmkuhl, S.; Theis, T.; Appelt, S.; Chekmenev, E. Y. Parahydrogen-Induced Radio Amplification by Stimulated Emission of Radiation. *Angew. Chem., Int. Ed.* **2020**, *132*, 8732−8738.
(26) Einstein, A. Zur quantentheorie der strahlung. *Phys. Z.* **1917**, *18*, 121−128.
(27) Appelt, S.; Kentner, A.; Lehmkuhl, S.; Blümich, B. From LASER physics to the para-hydrogen pumped RASER. *Prog. Nucl. Mag. Res. Spectrosc.* **2019**, *114*−*115*, 1−32.
(28) Appelt, S.; Lehmkuhl, S.; Fleischer, S.; Joalland, B.; Ariyasingha, N. M.; Chekmenev, E. Y.; Theis, T. SABRE and PHIP pumped RASER and the Route to Chaos. *J. Magn. Reson.* **2021**, *322*, No. 106815.
(29) Joalland, B.; Theis, T.; Appelt, S.; Chekmenev, E. Y. Background-Free Proton NMR Spectroscopy with Radiofrequency Amplification by Stimulated Emission Radiation. *Angew. Chem., Int. Ed.* **2021**, *60*, 26298−26302.
(30) Salnikov, O. G.; Trofimov, I. A.; Pravdivtsev, A. N.; Them, K.; Hövener, J.-B.; Chekmenev, E. Y.; Koptyug, I. V. Through-Space Multinuclear Magnetic Resonance Signal Enhancement Induced by Parahydrogen and Radiofrequency Amplification by Stimulated Emission of Radiation. *Anal. Chem.* **2022**, *94*, 15010−15017.
(31) Korchak, S.; Kaltschnee, L.; Dervisoglu, R.; Andreas, L.; Griesinger, C.; Glöggler, S. Spontaneous Enhancement of Magnetic Resonance Signals Using a RASER. *Angew. Chem., Int. Ed.* **2021**, *60*, 20984−20990.
(32) Lehmkuhl, S.; Fleischer, S.; Lohmann, L.; Rosen, M. S.; Chekmenev, E. Y.; Adams, A.; Theis, T.; Appelt, S. RASER MRI: Magnetic resonance images formed spontaneously exploiting cooperative nonlinear interaction. *Sci. Adv.* **2022**, *8*, No. eabp8483.
(33) Nelson, C.; Schmidt, A. B.; Adelabu, I.; Nantogma, S.; Kiselev, V. G.; Abdurraheem, A.; de Maissin, H.; Lehmkuhl, S.; Appelt, S.; Theis, T.; Chekmenev, E. Y. Parahydrogen-Induced Carbon-13 Radiofrequency Amplification by Stimulated Emission of Radiation. *Angew. Chem., Int. Ed.* **2023**, *62*, No. e202215678.
(34) Schmidt, A. B.; Berner, S.; Schimpf, W.; Müller, C.; Lickert, T.; Schwaderlapp, N.; Knecht, S.; Skinner, J. G.; Dost, A.; Rovedo, P.; Hennig, J.; von Elverfeldt, D.; Hövener, J. B. Liquid-state carbon-13 hyperpolarization generated in an MRI system for fast imaging. *Nat. Commun.* **2017**, *8*, 14535.
(35) Suefke, M.; Liebisch, A.; Blumich, B.; Appelt, S. External high-quality-factor resonator tunes up nuclear magnetic resonance. *Nat. Phys.* **2015**, *11*, 767−771.
(36) Ulmer, S.; Kracke, H.; Blaum, K.; Kreim, S.; Mooser, A.; Quint, W.; Rodegheri, C. C.; Walz, J. The quality factor of a superconducting RF resonator in a magnetic field. *Rev. Sci. Instrum.* **2009**, *80*, 123302.
(37) Zollitsch, C. W.; O'Sullivan, J.; Kennedy, O.; Dold, G.; Morton, J. J. L. Tuning high-Q superconducting resonators by magnetic field reorientation. *AIP Adv.* **2019**, *9*, 125225.
(38) Syms, R. R. A.; Floume, T.; Young, I. R.; Solymar, L.; Rea, M. Parametric Amplification of Magnetic Resonance Images. *IEEE Sens. J.* **2012**, *12*, 1836−1845.
(39) Nantogma, S.; Joalland, B.; Wilkens, K.; Chekmenev, E. Y. Clinical-Scale Production of Nearly Pure (>98.5%) Parahydrogen and Quantification by Benchtop NMR Spectroscopy. *Anal. Chem.* **2021**, *93*, 3594−3601.
(40) Chukanov, N. V.; Salnikov, O. G.; Shchepin, R. V.; Kovtunov, K. V.; Koptyug, I. V.; Chekmenev, E. Y. Synthesis of Unsaturated Precursors for Parahydrogen-Induced Polarization and Molecular Imaging of 1-^{13}C-Acetates and 1-^{13}C-Pyruvates via Side Arm Hydrogenation. *ACS Omega* **2018**, *3*, 6673−6682.
(41) Joalland, B.; Schmidt, A.; Kabir, M. S. H.; Chukanov, N. V.; Kovtunov, K. V.; Koptyug, I. V.; Hennig, J.; Hövener, J.-B.; Chekmenev, E. Y. Pulse-Programmable Magnetic Field Sweeping of Parahydrogen-Induced Polarization by Side Arm Hydrogenation. *Anal. Chem.* **2020**, *92*, 1340−1345.
(42) Joalland, B.; Chekmenev, E. Y. Scanning Nuclear Spin Level Anticrossings by Constant-Adiabaticity Magnetic Field Sweeping of Parahydrogen-Induced ^{13}C Polarization. *J. Phys. Chem. Lett.* **2022**, *13*, 1925−1930.
(43) Joalland, B.; Nantogma, S.; Chowdhury, M. R. H.; Nikolaou, P.; Chekmenev, E. Y. Magnetic Shielding of Parahydrogen Hyperpolarization Experiments for the Masses. *Magn. Reson. Chem.* **2021**, *59*, 1180−1186.

https://doi.org/10.1021/jacs.3c00776
J. Am. Chem. Soc. 2023, 145, 11121−11129